JGP Journal of General Physiology

ARTICLE

Rational design of a mutation to investigate the role of the brain protein TRIP8b in limiting the cAMP response of HCN channels in neurons

Alessandro Porro[1], Anna Binda[2], Matteo Pisoni[3], Chiara Donadoni[1], Ilaria Rivolta[2], and Andrea Saponaro[1]

TRIP8b (tetratricopeptide repeat–containing Rab8b-interacting protein) is the neuronal regulatory subunit of HCN channels, a family of voltage-dependent cation channels also modulated by direct cAMP binding. TRIP8b interacts with the C-terminal region of HCN channels and controls both channel trafficking and gating. The association of HCN channels with TRIP8b is required for the correct expression and subcellular targeting of the channel protein in vivo. TRIP8b controls HCN gating by interacting with the cyclic nucleotide-binding domain (CNBD) and competing for cAMP binding. Detailed structural knowledge of the complex between TRIP8b and CNBD was used as a starting point to engineer a mutant channel, whose gating is controlled by cAMP, but not by TRIP8b, while leaving TRIP8b-dependent regulation of channel trafficking unaltered. We found two-point mutations (N/A and C/D) in the loop connecting the CNBD to the C-linker (N-bundle loop) that, when combined, strongly reduce the binding of TRIP8b to CNBD, leaving cAMP affinity unaltered both in isolated CNBD and in the full-length protein. Proof-of-principle experiments performed in cultured cortical neurons confirm that the mutant channel provides a genetic tool for dissecting the two effects of TRIP8b (gating versus trafficking). This will allow the study of the functional role of the TRIP8b antagonism of cAMP binding, a thus far poorly investigated aspect of HCN physiology in neurons.

Introduction

In cortical and hippocampal pyramidal neurons, hyperpolarization-activated and cyclic nucleotide–gated (HCN) 1 subunits, the predominant HCN isoform, are selectively targeted to the distal regions of apical dendrites (Santoro et al., 1997; Magee, 1998; Lörincz et al., 2002). At these sites, the hyperpolarization-activated cation current (I_h) current generated by HCN channels controls dendritic excitability by filtering the integration of excitatory inputs (Magee, 1999; Williams and Stuart, 2000; Tsay et al., 2007; George et al., 2009). Aberrant regulation of HCN1 expression causes enhanced dendritic excitability, which, in turn, is associated with the development of temporal lobe epilepsy (Dubé et al., 2009; Shah et al., 2013). Therefore, both localization and function of HCN channels in the brain must be strictly and finely controlled.

To this end, HCN channels possess a regulatory subunit, TRIP8b (tetratricopeptide repeat–containing Rab8b-interacting protein), which is specifically expressed in the brain. TRIP8b tightly colocalizes with HCN1 in the distal dendrites of cortical and hippocampal pyramidal neurons (Santoro et al., 2004).

TRIP8b interacts with two different regions of the HCN C terminus: the C-terminal tripeptide SNL, a conserved sequence in HCN1, HCN2, and HCN4; and the cyclic nucleotide–binding domain (CNBD), also highly conserved among the three isoforms. Binding to the C-terminal SNL peptide is mediated by the tetratricopeptide repeat (TPR) domain, which is critical in controlling trafficking of HCN channels both in vitro and in vivo (Santoro et al., 2004, 2009, 2011; Piskorowski et al., 2011; Lewis et al., 2009). The precise channel distribution in the dendrites of both cortical and hippocampal neurons exactly matches that of TRIP8b and is lost in the TRIP8b-knockout mouse (Santoro et al., 2004, 2009; Piskorowski et al., 2011; Lewis et al., 2011), highlighting the crucial role of TRIP8b in the maintenance of appropriate HCN expression levels in these neurons.

A second interaction occurs between the HCN CNBD and the "core" region of TRIP8b, a central portion of ∼40 amino acids upstream of the TPR domain (Saponaro et al., 2018). TRIP8b, by competing with cAMP for binding to the CNBD, negatively shifts the voltage-dependent gating of HCN channels (Saponaro et al.,

[1]Department of Biosciences, University of Milano, Milano, Italy; [2]School of Medicine and Surgery, University of Milano-Bicocca, Monza, Italy; [3]Istituto Italiano di Tecnologia, Genova, Italy.

Correspondence to Andrea Saponaro: andrea.saponaro@unimi.it.

2018). This antagonistic effect was previously described as a mix of direct competition and allosteric inhibition (Hu et al., 2013). This postulated mechanism of interaction has been now supported by a structural model of the TRIP8b–HCN complex showing that TRIP8b interacts with the CNBD in two ways: (1) by directly competing with cAMP for binding to key residues on the C-helix; and (2) by binding to residues on a N-terminal loop connecting helix E′ to helix A, called N-bundle loop, that allosterically controls cAMP affinity (Saponaro et al., 2018).

Interestingly, the voltage dependency of HCN current gradually shifts to the left along the dendritic axis of pyramidal neurons (Magee, 1998, 1999). This gradient matches a similar gradient of TRIP8b expression in the same neurons and points to the fact that the same auxiliary subunit that controls channel distribution may also allow a fine tuning of its electrical properties.

In this respect, it would be useful to have an experimental tool able to dissect the two effects of TRIP8b on the channel in order to test the role of TRIP8b in modulating cAMP binding without altering expression and localization of the channel in the neuron. Identifying such mutations would allow to more effectively explore the role of TRIP8b in limiting the cAMP response of HCN channels in vivo.

A mutagenesis study on TRIP8b suggested that the trafficking effect exerted by the regulatory protein on HCN channels is mediated by its association with trafficking factors, whose binding sites are located in different regions of TRIP8b, including the two binding sites for HCN channels (TRIP8b$_{nano}$ sequence and TRP domain; Santoro et al., 2011). Therefore, an intact TRIP8b is necessary for the proper functioning of its trafficking effect. In order not to perturb the TRIP8b trafficking system, we thus decided to focus our attention on HCN channels. Furthermore, the CNBD region of HCN channels is well characterized both in term of its structure and function (Saponaro et al., 2014, 2018; Puljung et al., 2014; Zhou and Siegelbaum, 2007; Porro et al., 2019; Zagotta et al., 2003; Lolicato et al., 2011; Xu et al., 2010; Akimoto et al., 2014; Wainger et al., 2001) and thus represents a robust model system in which to search for the desired mutation.

To screen for such mutations, given the role of the CNBD C-helix in directly contacting cAMP, we focused our efforts on the N-bundle loop and proceeded to test candidate mutations for cAMP binding activity.

Here, we describe how we have identified a site-specific double mutation in the N-terminal bundle loop of HCN, which impairs TRIP8b binding to the CNBD but leaves the affinity for cAMP unaltered. Since the trafficking effect of TRIP8b on HCN is maintained, the mutation constitutes a valuable tool for future dissection of the multiple TRIP8b actions and for a characterization of the cAMP–TRIP8b regulatory system in vivo.

Materials and methods

Constructs

The cDNA encoding residues 235–275 (TRIP8b$_{nano}$) of murine TRIP8b (splice variant 1a-4) was previously cloned into pET-52b (EMD Millipore) bacterial expression vector (Saponaro et al., 2018). The cDNA encoding residues 521–672 of human HCN2 CNBD was previously cloned into a modified pET-24 (Saponaro et al., 2014) bacterial expression vector. The cDNA encoding full-length human HCN1 channel and mouse TRIP8b (1a-4) were cloned into the pcDNA 3.1 (Clontech Laboratories) mammalian expression vector. The cDNA encoding full-length mouse HCN2 was cloned in pCI (Promega) mammalian expression vector. Mutations were generated by site-directed mutagenesis (QuikChange site-directed mutagenesis kit; Agilent Technologies) and confirmed by sequencing.

Preparation of proteins

HCN2 CNBD WT and mutant proteins and TRIP8b$_{nano}$ WT and mutant peptides were produced and purified following the procedure previously described (Saponaro et al., 2014). Fig. S1 shows size-exclusion chromatography (SEC) profiles of HCN2 CNBD and TRIP8b$_{nano}$ WT and mutants performed as a final step of their purification procedure. SEC profiles were used to assess protein stability.

Isothermal titration calorimetry (ITC)

Measurements were performed at 25°C using a MicroCal VP-ITC microcalorimeter (Malvern Panalytical, ITC) following the procedure previously described (Saponaro et al., 2014, 2017; Saponaro, 2018).

Electrophysiology of HEK 293T cells

Cells were cultured and transfected following the procedure previously described (Saponaro et al., 2018; Porro et al., 2019). Whole-cell currents of HCN1 and HCN2 channels were recorded at room temperature 24 h after transfection either with a Dagan 3900A (Dagan Corporation) amplifier, or with an ePatch amplifier (Elements srl). For what concerns the data acquired with the Dagan 3900A amplifier, they were digitized with an Axon Digidata 1322A (Molecular Devices) converter. Voltage-clamp protocols are detailed in Saponaro et al. (2018). All data were analyzed offline with Axon pClamp 10.7 and Origin 16 (OriginLab Corp.) as detailed in Saponaro et al. (2018) and Porro et al. (2019).

Neuronal cell cultures and transfection

Primary cultures of cortical neurons were obtained from neonatal rats and cultured as previously reported (Binda et al., 2018; Bonzanni et al., 2018). Cortical neurons from human induced pluripotent stem cells (hiPSCs) were commercially available (iCell Neurons; Cellular Dynamic International) and cultured following manufacturer's instructions. Both types of neurons were transiently transfected using jetPRIME transfection reagent (Polyplus transfection; Euroclone) following manufacturer's instructions.

pcDNA3.1 vector containing 1 µg cDNA of either WT or mutant HCN1 channels was cotransfected with a plasmid containing cDNA of GFP (0.3 µg) for transient expression. For coexpression with TRIP8b (1a-4), neurons were transiently transfected with 1 µg cDNA of either WT or mutant HCN1 channels, 1 µg cDNA of TRIP8b (1a-4) WT, and 0.3 µg cDNA of GFP.

Electrophysiology of neuronal cell cultures

Whole-cell patch-clamp experiments were performed at room temperature 48 h after transfection (Bonzanni et al., 2018).

GFP-positive neurons were selected for the recording. The extracellular solution was composed as follows (in mM): 140 NaCl, 5.4 KCl, 1.8 $CaCl_2$, 1 $MgCl_2$, 5.5 D-glucose, and 5 HEPES-NaOH, pH 7.4. During whole-cell recording, the perfusing solution was switched to a high-K^+ solution containing (in mM) 110 NaCl, 0.5 $MgCl_2$, 1.8 $CaCl_2$, 5 HEPES-NaOH, 30 KCl, 1 $BaCl_2$, 2 $MnCl_2$, and 0.1 NiCl, pH 7.4. The intracellular-like solution contained (in mM) 130 KCl, 10 NaCl, 1 EGTA-KOH, 0.5 $MgCl_2$, 2 ATP (Na_2-salt), 5 creatine phosphate, 0.1 GTP (Na_2-salt), and 5 HEPES-KOH, pH 7.2. From a holding potential of −30 mV, hyperpolarizing steps in the range of −20 to −120 mV followed by a fully activating step at −120 mV were applied to measure activation curves in standard two-step protocols. Single activation curves were fitted to the Boltzmann equation $y = 1/\{1 + \exp[(V - V_{1/2})/s]\}$, where V is voltage, $V_{1/2}$ is half-maximum activation potential, and s is the inverse slope factor, to yield $V_{1/2}$ and s values, which were then averaged (DiFrancesco, 1999). The current–voltage relationship curves were obtained normalizing the current amplitude at each step tested by the cell capacitance and plotting the current density obtained versus the voltage test pulse. Activation and deactivation time constants (τ) were obtained by fitting a single exponential function, $I = I0\exp(-t/\tau)$, to current traces obtained with the activation protocol described above. Deactivation time constants were obtained by fitting tail currents collected at −40 mV after a fully activation pulse at −130 mV.

Statistical analysis

Statistical significance was assessed with one-way ANOVA, followed by post-hoc Tukey or Fisher tests where applicable. The α level was set to 0.05 for all statistical analysis. All analyses were performed using Origin 16 (OriginLab Corp.).

Online supplemental material

Fig. S1 shows representative SEC profiles of His_6-MBP–tagged human HCN2 CNBD and Strep-tagged $TRIP8b_{nano}$ WT and mutants performed to assess protein stability. These proteins were used for ITC assays related to Figs. 2 and 4 and Table 1. Fig. S2 shows the structure of human HCN2 CNBD and emphasizes the N-bundle loop, the structural element where the double mutation NA/DC is located. Fig. S3 shows the electrophysiological assay performed to test the cAMP sensitivity of mouse HCN2 NA/DC mutant channels.

Results

Identification of a mutation that impairs TRIP8b binding to CNBD but not cAMP

The interaction of TRIP8b with the HCN channel's CNBD has been characterized at atomic level by an NMR-based model structure of the complex formed by human HCN2 CNBD and $TRIP8b_{nano}$, a 40–amino acid–long peptide that constitutes the minimal binding unit of TRIP8b to the CNBD (Fig. 1 A). The complex is formed mainly by electrostatic interactions, with $TRIP8b_{nano}$ contributing negative and CNBD positive charges. $TRIP8b_{nano}$ establishes salt bridges in two sites of the CNBD C-helix: (1) residues K666, K665, and R662 (site I); and (2) residue R650 (site II). $TRIP8b_{nano}$ further interacts with the CNBD in a third point, at the level of the N-bundle loop, forming a hydrogen bond with N547 (site III).

We have previously validated the model of the CNBD–$TRIP8b_{nano}$ complex by showing that reversing (K666E, K665E, and R662E) or introducing (N547D) a charge in these positions strongly reduces the binding affinity for $TRIP8_{nano}$, presumably due to electrostatic repulsion with the negatively charged residues of $TRIP8b_{nano}$ (Saponaro et al., 2018).

In the search for a mutation that disrupts TRIP8b, but not cAMP, binding, we first checked the affinity for cAMP in the above mutants. Since HCN2 is very sensitive to cAMP (Lolicato et al., 2011; Wainger et al., 2001), we decided to use this isoform to screen for mutations that did not perturb cAMP binding and efficacy.

Of the three mutants at site I, we picked K666E, but not K665E and R662E. R662E was discarded because R662 directly contacts cAMP in the crystal structure of CNBD (Zagotta et al., 2003; Lolicato et al., 2011; Fig. 1 B). K665E was not tested because it was previously shown that alanine substitution of the corresponding K638 in mHCN2 channels already alters cAMP sensitivity (Zhou and Siegelbaum, 2007).

Affinity of K666E for cAMP was evaluated by ITC. Fig. 2, A and B show heat exchanges obtained by injecting cAMP (titrant) into the chamber containing either WT or K666E CNBD (titrands), respectively. The binding curve was obtained by integrating the peaks (upper panels) and plotting the values as a function of the molar ratio between titrant and titrand (lower panels). By fitting a single binding site model to the data (red solid line), we calculated the average K_d values ($n = 3$ repetitions) reported in Table 1. The mutant shows a threefold decreased affinity for cAMP compared with the WT (K666E = 6.3 ± 0.3 μM; WT = 1.9 ± 0.1 μM). The reduction in cAMP affinity is moderate but significant (Table 1).

Next, we tested R650E, which controls $TRIP8b_{nano}$ binding at site II. This residue does not directly contact the cAMP binding pocket and was therefore considered a promising candidate for our purpose. ITC analysis (Fig. 2 C) shows an even more moderate, though still significant, change in cAMP affinity with respect to the control CNBD. The mean K_d value is 1.9 ± 0.1 μM for WT and 4 ± 0.1 μM for the mutant (Table 1).

In our experience, moderate changes in the K_d, like the ones we measured by ITC for K666E and R650E mutants, may have a likewise modest but significant effect when tested in electrophysiology.

As a precaution, we therefore decided to test whether R650E mutation, which caused the most moderate reduction of cAMP affinity in the isolated CNBD (Fig. 2 C and Table 1), could significantly affect cAMP sensitivity also in the full-length channel. Mouse HCN2 R632E (corresponding to R650E) was transiently expressed in HEK 293T cells and its currents recorded by patch clamp in the absence and in the presence of 5 μM cAMP in the patch pipette. Fig. 3 A shows a comparison of representative currents elicited by WT and mutant channels, respectively. Fig. 3 B shows the mean activation curves of the two channels obtained from the analysis of currents in A and other cells ($n \geq 10$). Activation curves were obtained from tail currents recorded at −40 mV, normalized for the cell capacitance and plotted as a

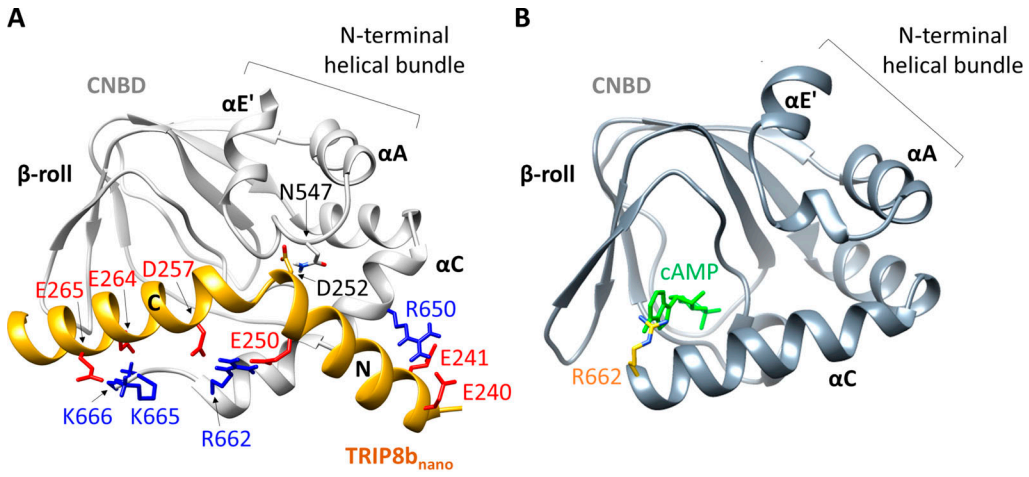

Figure 1. **The HCN CNBD–TRIP8b$_{nano}$ complex. (A)** Ribbon representation of the NMR-based model structure of the complex between human HCN2 CNBD (light gray) and TRIP8b$_{nano}$ (gold). The structural elements of both proteins involved in the binding are labeled as follows: for the CNBD, E′-helix (αE′) and A-helix (αA), which form, together with their inter-helical loop, the N-terminal helical bundle; C-helix (αC); for TRIP8b$_{nano}$, helix N (N) and helix C (C). Negatively charged residues of TRIP8b$_{nano}$ and positively charged residues of CNBD (αC), which are involved in the electrostatic interaction, are shown as sticks, labeled and colored in red and blue, respectively. D252 of TRIP8b$_{nano}$ and N547 of the N-bundle loop and are shown as sticks and labeled. **(B)** Ribbon representation of human HCN2 CNBD (dark gray) bound to cAMP (PDB accession no. 3U10). cAMP (green stick) is shown within its binding pocket composed by the β-roll and the distal region of α helix C, which acts as a lid and closes cAMP within the β-roll. Residue R662 (yellow stick) of α helix C, which contacts cAMP, is shown. The structural elements of CNBD are labeled.

function of the preconditioning voltage. Fitting data to a Boltzmann equation (solid lines of Fig. 3 B; see Materials and methods for the equation) yielded the half-activation potentials ($V_{1/2}$; Fig. 3 C). The mutant channel shows no difference in $V_{1/2}$ in control solution (WT = −96.1 ± 0.5 mV; mutant = −96.4 ± 0.4 mV) but appears slightly less responsive to cAMP than the WT channel (WT = −84 ± 0.4 mV; mutant = −86.9 ± 0.4 mV). On average, the shift induced by 5 µM cAMP on $V_{1/2}$ is 12.1 ± 0.6 mV for the WT and 9.5 ± 0.6 mV for the mutant channel. This effect was considered nonnegligible. Given the fact that the reduction in cAMP binding/response due to R650E (R632E in mHCN2) was confirmed to be moderate but significant in two different experimental conditions (Fig. 3 and Table 1), we decided to look for other possible mutants in site III.

The crucial residue of site III, N547, is in the loop connecting helix E′ of the C-linker to helix A at the N-terminus of the CNBD (N-bundle loop; Fig. 1 A). The loop is a crucial regulatory point of the channel, as it mechanically connects the CNBD to the C-linker. Upon cAMP binding to the CNBD, the loop forms a new helix (F′) that moves upward together with helices E′ and A, the so-called N-terminal helical bundle, thus propagating cAMP signal from the CNBD to the rest of the protein via the C-linker (Saponaro et al., 2014; Lee and MacKinnon, 2017; Li et al., 2017). Our previous finding that mutation N547D disrupts not only TRIP8$_{nano}$ but also cAMP binding (Saponaro et al., 2018) underscored a previously unaddressed role of the N-bundle loop in allosterically modulating cAMP binding to the CNBD.

As the N547D mutation did not satisfy our criteria for isolating TRIP8b binding from cAMP binding activity, we considered alternative mutations. Interestingly, the closely related CNG channels, which bind to cAMP like HCN channels but do not bind to TRIP8b (Santoro et al., 2011), carry an aspartate instead of asparagine at the position corresponding to N547, just like the N547D mutant. The aspartate in CNG is however followed by a second substitution within an otherwise highly conserved sequence, namely a cysteine instead of alanine (Fig. S2). To fully mimic the CNG channel sequence, we thus introduced a double point mutation in our HCN CNBD construct. Binding assays performed by ITC show that the HCN CNBD N547D/A548C mutant (hereafter NA/DC) displays a 6-fold decrease in the affinity for TRIP8b$_{nano}$ (compare Fig. 4 A to Fig. 4 C; Table 1). In contrast, the affinity for cAMP of the double mutation remains essentially unaltered (Fig. 2 D and Table 1), as expected from the homology with CNG channels. Importantly, the decrease of TRIP8b$_{nano}$ binding activity due to the NA/DC mutation in the CNBD (Fig. 4 C and Table 1) was largely rescued by pairing CNBD NA/DC mutant with the D252N point mutation in TRIP8b$_{nano}$ (Fig. 4 D and Table 1). The results of this swap experiment provide further demonstration that the NA/DC double mutant is appropriately folded and strongly support an interaction between residues in the CNBD N-bundle loop and the bend region between helix N and helix C of TRIP8b$_{nano}$, as predicted by our model (Fig. 1 A). It is worth noting that TRIP8b$_{nano}$ D252N mutant did not affect binding to CNBD (Fig. 4 B and Table 1), presumably because the added asparagine residue can develop hydrophilic contacts with N547 of CNBD.

Having demonstrated that the NA/DC double mutation affects TRIP8b, but not cAMP, binding to the isolated HCN2 CNBD, for completeness, we showed that cAMP response is unaltered also in the full-length HCN2 channel upon introduction of the NA/DC mutation (Fig. S2 and Fig. S3).

NA/DC mutation in the full-length channel

Considering these findings, we next tested whether the NA/DC double mutation may also be able to affect TRIP8b binding (but not cAMP binding) in the context of a full-length channel.

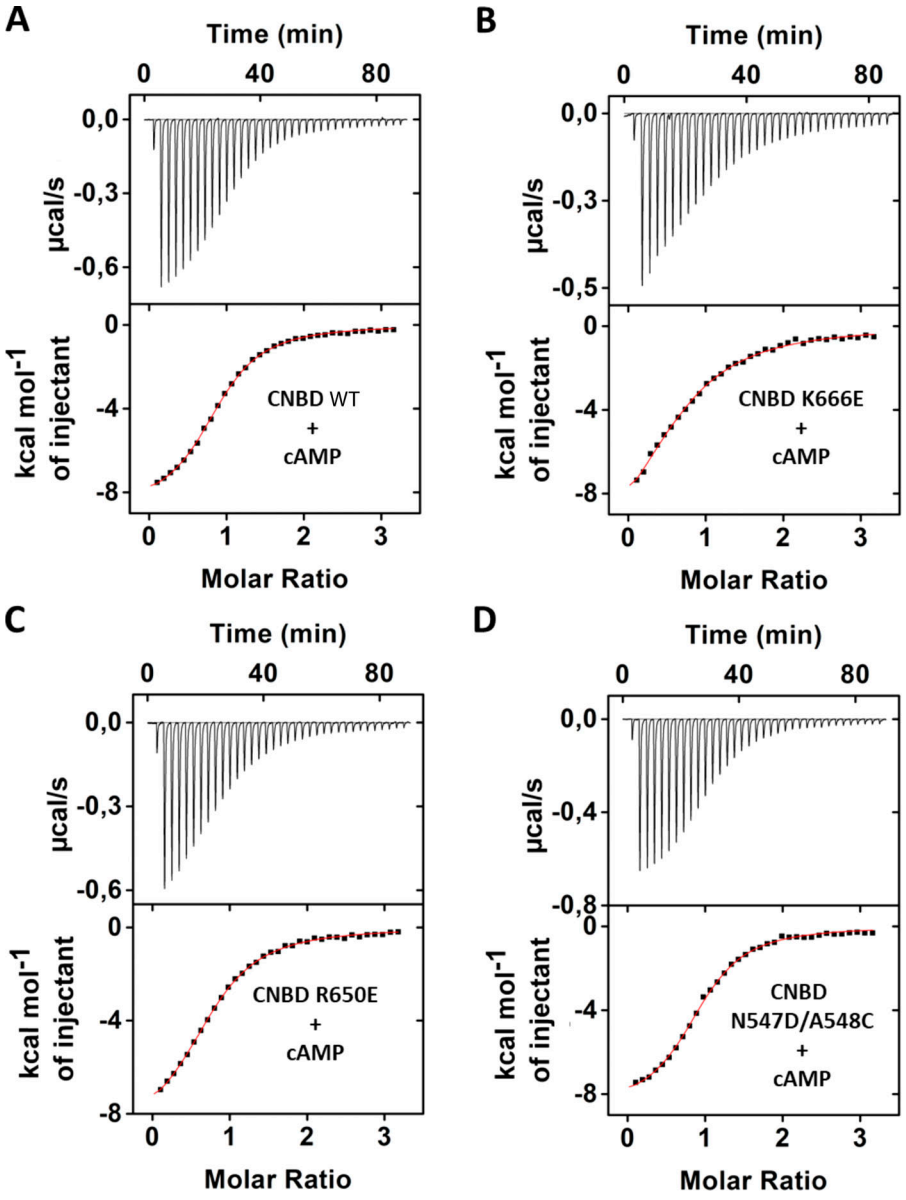

Figure 2. **In vitro analysis of CNBD–cAMP interaction.** Examples of binding of cAMP to His_6-MBP-tagged human HCN2 CNBD WT (A) and mutants (B–D) measured by ITC. Top: Heat changes (µcal/s) during successive injections of 8 µl of the corresponding cAMP (200 µM) into the chamber containing CNBD (20 µM). Bottom: Binding curve obtained from data displayed in the upper panel. The peaks were integrated, normalized to cAMP concentration, and plotted against the molar ratio (cAMP/CNBD). Solid red line represents a nonlinear least-squares fit to a single-site binding model (see Materials and methods).

The motivation for searching for the NA/DC mutation is to use it in physiological contexts in vivo as a genetic tool to dissect the two effects of TRIP8b (gating versus trafficking) on HCN channels. Therefore, we focused our attention on HCN1, given the well-characterized interaction between this HCN isoform and TRIP8b in neurons. We thus introduced the mutation in HCN1 channels, the predominant HCN isoform in cortical and hippocampal pyramidal neurons, whose gating and trafficking are controlled by TRIP8b both in vitro and in vivo (Santoro et al., 2009; Piskorowski et al., 2011; Lewis et al., 2009, 2011). Moreover, we coexpressed HCN1 channels with TRIP8b splice variant 1a-4, as this is the predominant isoform in the forebrain and is crucial for the proper localization of HCN1 in pyramidal neurons (Santoro et al., 2009; Piskorowski et al., 2011).

The mutation in HCN1 channels, by preventing TRIP8b binding to CNBD, may result in a selective inhibition of the gating regulation without affecting the trafficking regulation. Indeed, it is worth remembering that TRIP8b (1a-4) exerts its effect on channel trafficking mainly by means of the TPR domain, which is not involved in the binding to CNBD (Santoro et al., 2011).

We therefore recorded currents from HEK 293T cells transiently transfected with HCN1 alone or together with TRIP8b (1a-4; Fig. 5 A). Fig. 5 B shows the activation curves obtained from tail currents recorded at −40 mV (see arrow in Fig. 5 A), normalized for the cell capacitance and plotted as a function of the preconditioning voltage. The half-activation potential ($V_{1/2}$), yielded from the fitting of the data to the Boltzmann equation (solid and dashed lines of Fig. 5 B; see Materials and methods for equation), is plotted in Fig. 4 C. Fig. 5 D shows maximal current density values calculated at the saturating voltage of −120 mV (see arrowhead in Fig. 5 B).

Because of its higher affinity for cAMP compared with the other HCN isoforms, the HCN1 isoform shows virtually a fully rightward shifted activation curve due to the endogenous cAMP levels present in HEK 293T cells (Saponaro et al., 2018). When

Table 1. **cAMP and TRIP8b$_{nano}$ binding to CNBD**

Titrant	CNBD (titrad)	K_d ± SEM (μM)	P value (compared to WT)	n
cAMP	WT	1.9 ± 0.1	—	3
	R650E	4 ± 0.1	3.2E-04	3
	K665E	6.3 ± 0.3	1.2E-06	3
	N547D/A548C	1.8 ± 0.1	0.98	3
TRIP8b$_{nano}$ WT	WT	1.3 ± 0.1	—	3
TRIP8b$_{nano}$ D252N	WT	3.5 ± 0.5	0.1	3
TRIP8b$_{nano}$ WT	N547D/A548C	9.3 ± 0.9	4.8E-5	3
TRIP8b$_{nano}$ D252N	N547D/A548C	3.6 ± 0.6	0.09	3

ITC measurements of cAMP and Strep-tagged TRIP8b$_{nano}$ (WT and mutant) binding to His$_6$-MBP–tagged human HCN2 CNBD (WT and mutants). Data are reported as mean ± SEM. Statistical analysis performed with one-way ANOVA, followed by post-hoc Tukey test.

TRIP8b (1a-4) is cotransfected with HCN1, the $V_{1/2}$ of the channel is shifted significantly to more hyperpolarized potentials (HCN1 WT = −72.7 ± 0.4 mV; HCN1 WT + TRIP8b (1a-4) = −78.2 ± 0.5 mV; Fig. 5, B and C). This reflects the fact that TRIP8b prevents cAMP binding to the channel. This negative shift in the activation curve closely matches the shift recorded with the HCN1 R549E cAMP-insensitive mutant, which essentially prevents cAMP binding (Chen et al., 2001; Saponaro et al., 2018), suggesting that TRIP8b fully antagonizes the interaction of endogenous cAMP with the channel.

It is worth noting that whole-cell configuration was preferred over inside-out because of the known tendency of TRIP8b to dissociate from HCN1 upon patch excision (Santoro et al., 2009). It is therefore possible that the control condition does not strictly represent the currents in the complete absence cAMP.

As noted in previous studies (Lewis et al., 2009; Santoro et al., 2009), cotransfection of TRIP8b (1a-4) has also a second effect on HCN1 channel function, namely an ∼2.5-fold increase in maximal current density (Fig. 5, B and D).

We thus introduced the NA/DC double mutation in the background of the full-length human HCN1 channel (N478D/A479C). Consistent with its effect on the isolated CNBD fragment, the double mutant had a rightward shifted $V_{1/2}$ identical to the WT HCN1 channel (HCN1 NA/DC = −72.6 ± 0.6 mV; Fig. 5, B and C). This confirms an intact response of the mutant to endogenous cAMP and shows, quite strikingly, that cotransfection with TRIP8b (1a-4) was completely ineffective in preventing the facilitatory effect of cAMP on channel activation (HCN1 NA/DC + TRIP8b (1a-4) = −73.2 ± 0.4 mV; Fig. 5, B and C). It is worth noting that TRIP8b decreases the kinetics of channel opening, while increasing the kinetics of channel closing (Santoro et al., 2009). As expected, the presence of TRIP8b significantly reduced the time constants of HCN1 current activation, while accelerating the time constant of deactivation (Fig. 5 E and Table 2). The NA/DC double mutation, by impairing the TRIP8b-

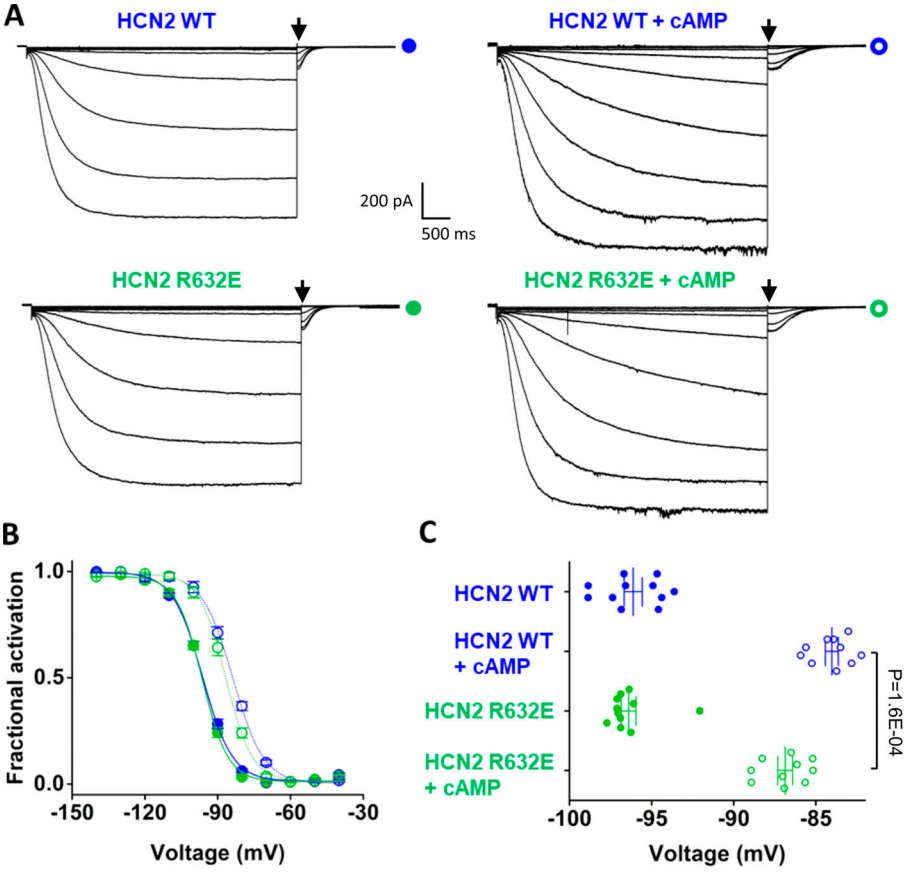

Figure 3. **cAMP sensitivity of HCN2 R632E channel. (A)** Representative whole-cell current traces of mouse HCN2 WT (top) and R632E mutant (bottom) recorded in HEK 293T cells transiently expressing the channels with control solution (left) or with 5 μM cAMP (right) in the patch pipette. Arrows indicate the currents selected for analysis in B. **(B)** Normalized mean activation curves of HCN2 WT in control solution (blue filled circle) and cAMP (blue open circle) and HCN2 R632E in control solution (green filled circle) and cAMP (green open circle) obtained from tail currents collected at −40 mV (see arrows in A). Lines show data fit to a Boltzmann function (see Materials and methods), from which we derived the half-activation potentials ($V_{1/2}$) plotted in C. **(C)** Mean half-activation potential ($V_{1/2}$) of HCN2 WT in control solution (blue filled circle) = −96.3 ± 0.4 mV; HCN2 WT with cAMP (blue open circle) = −83.7 ± 0.3 mV; HCN2 R632E in control solution (green filled circle) = −96.4 ± 0.3 mV; HCN2 R632E with cAMP (green open circle) = −86.7 ± 0.3 mV. Data are plotted as dots and the line represents the mean value ± SEM. The number of cells was ≥10. Statistical analysis performed with one-way ANOVA, followed by post-hoc Tukey test (P values are denoted within the scatterplot graph).

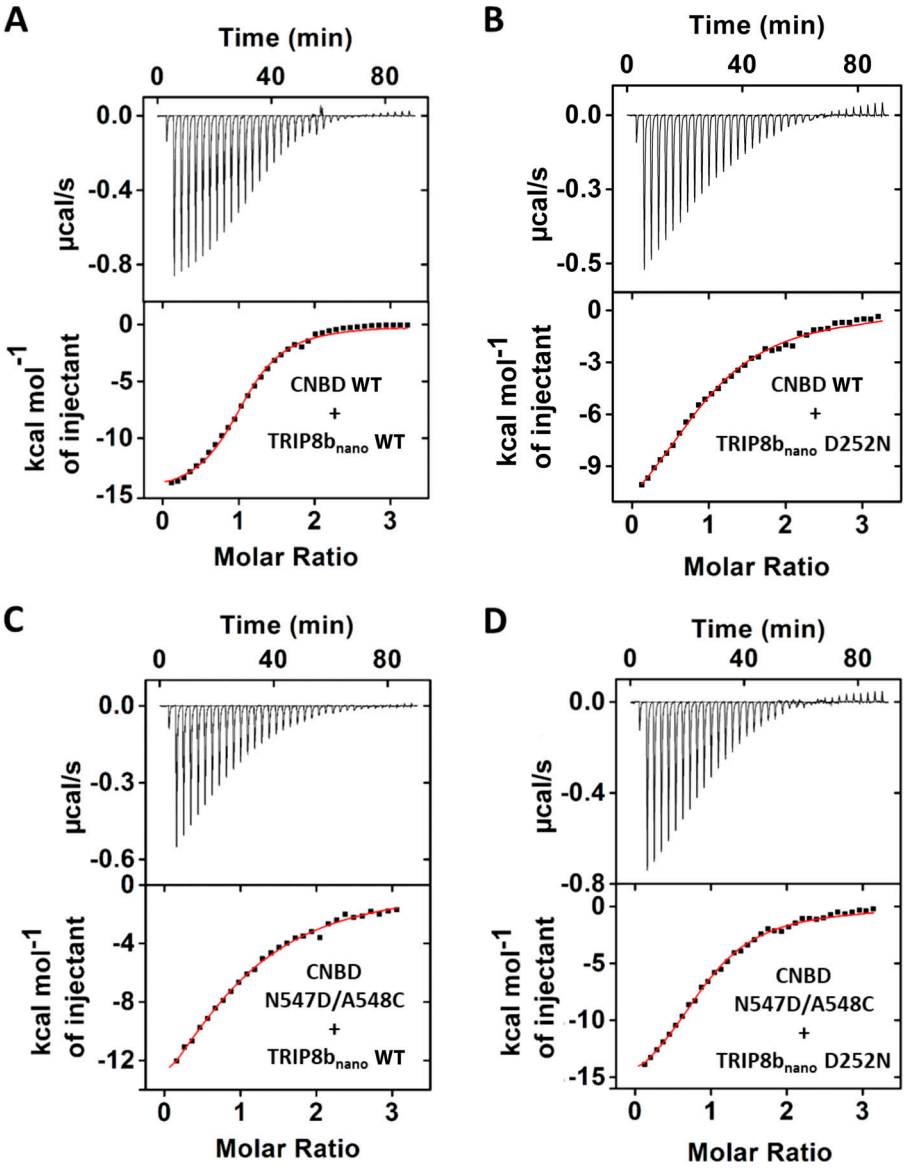

Figure 4. **In vitro analysis of CNBD–TRIP8b$_{nano}$ interaction. (A–D)** Examples of binding of Strep-tagged TRIP8b$_{nano}$ (WT and mutants) to His6-MBP-tagged human HCN2 CNBD (WT and mutants) measured by ITC. Top: Heat changes (µcal/s) during successive injections of 8 µl of the corresponding TRIP8b$_{nano}$ (200 µM) into the chamber containing CNBD (20 µM). Bottom: Binding curve obtained from data displayed in the top panel. The peaks were integrated, normalized to TRIP8b$_{nano}$ concentration, and plotted against the molar ratio (TRIP8b$_{nano}$/CNBD). Solid red line represents a nonlinear least-squares fit to a single-site binding model (see Materials and methods).

dependent regulation of HCN1 gating, impaired also its ability to modulate HCN1 kinetics (Fig. 5 E and Table 2).

At the same time, TRIP8b still exerted its normal positive effect on channel surface expression, as reflected by the increase in maximal current density of the mutant channel, which is comparable to WT (Fig. 5, B and D).

In conclusion, the double mutation NA/DC in the HCN CNBD is enough to prevent the effect of TRIP8b on cAMP, while having no impact on the role of TRIP8b to promote channel expression and trafficking. Based on these results, we reckoned the double mutation may be employed as a genetic tool for dissecting TRIP8b actions (gating versus trafficking) on HCN channels.

NA/DC mutation in the physiological context of neurons

We next tested the effect of the NA/DC mutant in the more physiological context of neurons. As proof of principle, we first employed primary cultures of cortical neurons from neonatal rats. These cells were transiently transfected with HCN1 (WT or NA/DC mutant) alone, or together with TRIP8b (1a-4).

Based on the results in HEK 293T cells, we expected the NA/DC mutation to prevent TRIP8b-induced effects on gating, but not on trafficking. Fig. 6 A shows representative currents recorded from cells transfected with HCN1 WT or NA/DC, with or without TRIP8b (1a-4). As expected, regardless of the double mutation, TRIP8b (1a-4) exerted its normal positive effect on channel surface expression, as it increased the current density roughly to the same extent in both WT and NA/DC (~2.3- and 2.2-fold increase, respectively; Fig. 6 B and Table 3).

Co-transfection with TRIP8b significantly left shifted the HCN1 WT activation curve ($V_{1/2}$ = −81.9 ± 1.4 mV for HCN1 WT; $V_{1/2}$= −88.6 ± 1.1 mV HCN1 WT + TRIP8b (1a-4); Fig. 6, C and D), indicating that TRIP8b prevents cAMP binding to the channel also in the native context of cortical neurons, and that basal cAMP levels in these cells are sufficiently high to fully activate the channel in the absence of TRIP8b.

Consistent with the effect shown in HEK 293T cells, the NA/DC mutant had a rightward shifted $V_{1/2}$ identical to the WT HCN1 channel ($V_{1/2}$ = −82.4 ± 1 mV; Fig. 6, C and D). This

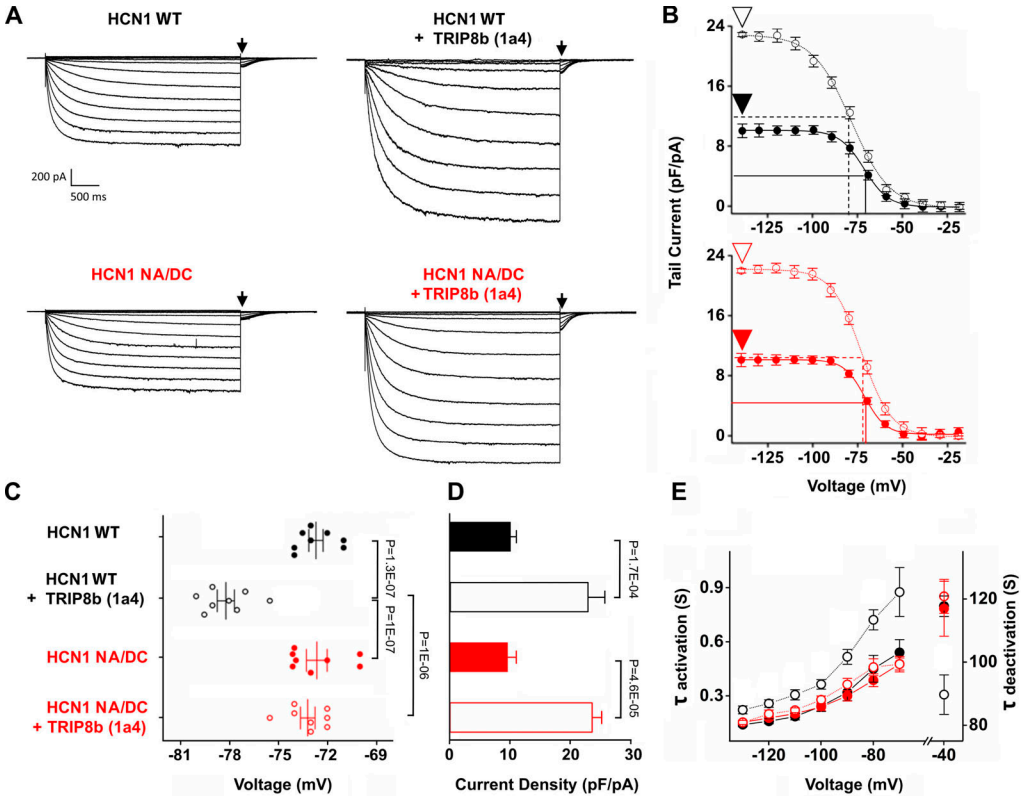

Figure 5. **The NA/DC double mutation in HCN1 prevents TRIP8b regulation of channel function**. **(A)** Representative whole-cell current traces of human HCN1 WT (top) and N478D/A479C (NA/DC) mutant (bottom) recorded in HEK 293T cells transiently expressing the channels alone (left) or with TRIP8b (1a-4; right) and analyzed as described in Materials and methods. Arrows indicate the current selected for analysis in B. **(B)** Mean activation curves of HCN1 WT (black filled circle), HCN1 WT + TRIP8b (1a-4; black open circle), HCN1 NA/DC (red filled circle), and HCN1 NA/DC + TRIP8b (1a-4; red open circle) channels obtained from tail currents collected at −40 mV (see arrows in A). The currents were normalized for the cell capacitance and plotted (changed in sign) as a function of test voltages. Solid and dashed lines indicate the half-activation potential ($V_{1/2}$) value, while arrowheads indicate the current density value at saturation, plotted respectively in C and D. **(C)** Mean half-activation potential ($V_{1/2}$) of HCN1 WT (black filled circle) = −72.7 ± 0.4 mV; HCN1 WT + TRIP8b (1a-4; black open circle) = −78.2 ± 0.5 mV; HCN1 NA/DC (red filled circle) = −72.6 ± 0.6 mV; and HCN1 NA/DC + TRIP8b (1a-4; red open circle) = −73.2 ± 0.4 mV. P values are denoted within the scatter plot graph. **(D)** Mean maximal tail current density of HCN1 WT (black filled bar) = 10.1 ± 2.7 pA/pF; HCN1 WT + TRIP8b (1a-4; black open bar) = 23 ± 8 pA/pF; HCN1 NA/DC (red filled bar) = 9.6 ± 4 pA/pF; and HCN1 NA/DC + TRIP8b (1a-4; red open bar) = 23.8 ± 4.5 pA/pF. P values are denoted within the column bar graph. **(E)** Mean activation and deactivation time constants (before and after the x-axis break, respectively) of HCN1 WT (black filled circle), HCN1 WT + TRIP8b (1a-4; black open circle), HCN1 NA/DC (red filled circle), and HCN1 NA/DC + TRIP8b (1a-4; red open circle). Time constant of activation and deactivation were calculated, as described in Materials and methods. All values and exact P values are reported in Table 2. Data are plotted as a dot and the line represents the mean value ± SEM. *n* = 8 cells. Statistical analysis performed with one-way ANOVA, followed by post-hoc Tukey test.

confirms an intact response of the mutant to endogenous cAMP. Strikingly, TRIP8b (1a-4) was completely ineffective in preventing the facilitatory effect of cAMP on the activation of mutant channel ($V_{1/2}$ = −82.2 ± 1.2 mV; Fig. 6, C and D). Considering the current density at −120 mV of mock-transfected neurons (−10.6 ± 1.8 pA/pF, *n* = 25) and its comparison with the HCN1-transfected ones (see Table 3), we can conclude that the contribution of endogenous HCN, presumably HCN1 (Battefeld et al., 2012), and TRIP8b, is truly negligible.

To maintain the complexity of the neuronal background and, at the same time, analyze the behavior of the double HCN1 mutant in a human system, we turned our attention to cortical neurons derived from hiPSCs.

Despite the fact that the measured currents were smaller in this system (Fig. 7, A and B), the coexpression of TRIP8b (1a-4) with HCN1 channels induced an increase of ∼2.5-fold in the current density of both WT and NA/DC mutant (Fig. 7, A and B; and Table 4), the same extent of the increase measured in rat cortical neurons.

Once again, the presence of TRIP8b induced a significant negative shift in the activation curve of HCN1 WT compared with the mutant channel (Fig. 7 C; $V_{1/2}$ = −85.1 ± 1.9 mV for WT; $V_{1/2}$ = −79.9 ± 1.7 mV for the mutant; P = 0.034). It is worth noting that when HCN1 channels (both WT and mutant) are expressed alone we could not carefully measure activation curves because of the low current density. On the contrary, TRIP8b, by increasing channel surface expression, allowed us to properly analyze activation curves (Fig. 7 C). Nonetheless, considering the data gathered in the other cellular systems and that, contrary to HCN1 WT, the activation curve of NA/DC is insensitive to TRIP8b (Fig. 7 C), we assume that human derived-cortical neurons HCN1 WT and NA/DC mutant possess the same sensitivity for endogenous cAMP.

Taken together, these findings indicate that NA/DC mutation exerts its inhibitory effect on the TRIP8b-dependent control of HCN channel gating, while leaving unaffected the regulation of trafficking and expression, even in the more physiological context of cultured cortical neurons.

Table 2. **Mean activation and deactivation time constants of HCN1 WT and NA/DC mutant in the presence and absence of TRIP8b (1a-4)**

V/mV		HCN1 WT	HCN1 WT+ TRIP8b	P value	HCN1 NA/DC	HCN1 NA/DC + TRIP8b	P value
−70	τ activation (ms)	540.5 ± 71.3	875.7 ± 135.3	4.1E−03	477.2 ± 33.1	476.2 ± 42.8	1.0
−80		450.5 ± 74.4	721.1 ± 55.7	3.8E−03	386.6 ± 35.8	459.3 ± 46.7	0.4
−90		319.4 ± 46.3	516.4 ± 41.0	2.3E−03	299.6 ± 28.5	363.5 ± 34.2	0.25
−100		242.5 ± 28.9	364.0 ± 26.7	3.15E−03	238.8 ± 20.9	278.1 ± 21.0	0.3
−110		185.4 ± 18.4	305.6 ± 28.0	7.5E−03	201.4 ± 14.9	220.4 ± 13.0	0.4
−120		159.3 ± 13.2	257.6 ± 20.4	3.9E−03	177.9 ± 12.2	199.6 ± 21.6	0.4
−130		141.2 ± 11.4	221.9 ± 21.9	6.4E−04	153.5 ± 9.9	152.7 ± 11.2	1.0
−40	τ deactivation (ms)	117.7 ± 3.2	89.7 ± 6.2	7.7E−03	116.9 ± 8.7	120.8 ± 5.3	0.7

Data are reported as mean ± SEM. Statistical analysis performed with one-way ANOVA, followed by post-hoc Tukey test.

As in the case of rat cortical neurons, we could not exclude the presence of endogenous HCN1 and TRIP8b proteins in hiPSC-derived neurons. Nonetheless, considering that HCN1 current recorded from transfected neurons was about three time higher than the current recorded from mock-transfected cells (mean current density at −120 mV of HCN1 WT −27.2 ± 7.7 pA/pF; mean current density at −120 mV of mock-transfected neurons −10.4 ± 2.8 pA/pF) potential contribution of the endogenous I_h current can be considered minimal.

Discussion

Guided by the molecular model described in Saponaro et al. (2018) and illustrated here in Fig. 1 A, we identified and characterized the double mutation N547D/A548C in the

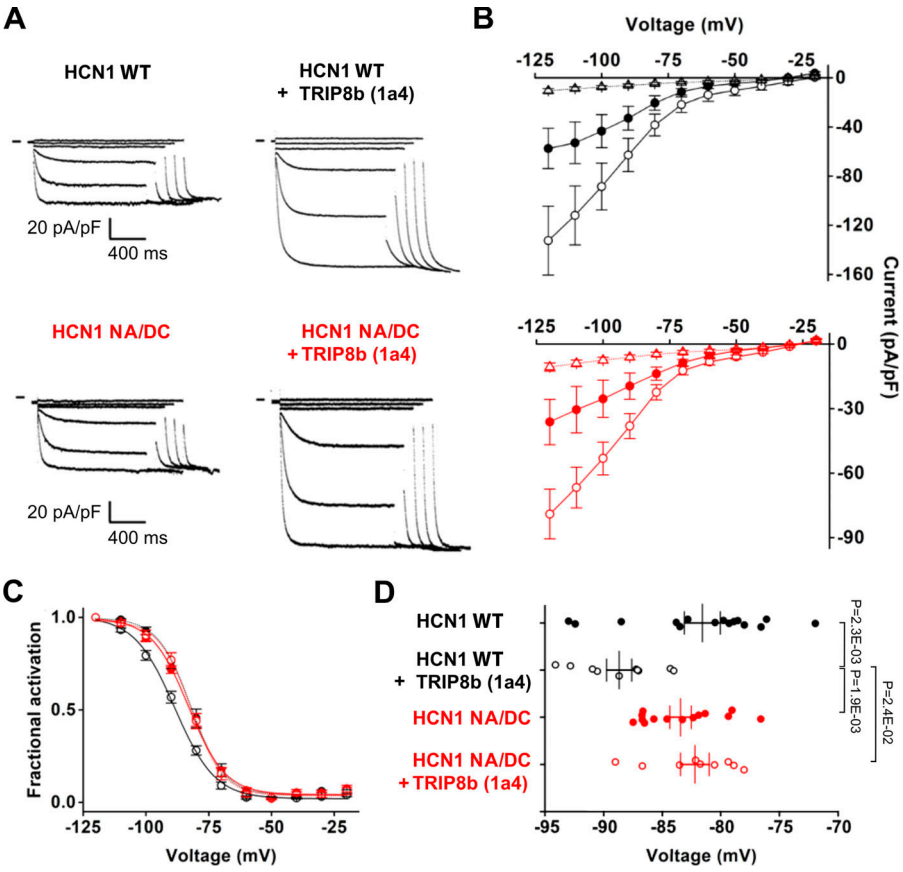

Figure 6. **The NA/DC double mutation prevents TRIP8b regulation of HCN1 gating in cortical neurons from neonatal rats. (A)** Representative whole-cell current traces of human HCN1 WT (top) and N478D/A479C (NA/DC) mutant (bottom) recorded in primary cultures of cortical neurons from neonatal rats transiently expressing the channels alone (left) or with TRIP8b (1a-4; right) and analyzed as described in Materials and methods. **(B)** Top: Mean current–voltage relationship of HCN1 WT (black filled circle) and HCN1 WT + TRIP8b (1a-4; black open circle). Bottom: Mean current–voltage relationship of HCN1 NA/DC (red filled circle) and HCN1 NA/DC + TRIP8b (1a-4; red open circle). Empty triangles in both panels represent the current recorded in the mock-transfected neurons. Mean current density (pA/pF) measured at −120 mV of HCN1 WT = −57.5 ± 16.3 pA/pF; HCN1 WT + TRIP8b (1a-4) = −132.4 ± 28 pA/pF; HCN1 NA/DC = −36.3 ± 10.5 pA/pF; and HCN1 NA/DC + TRIP8b (1a-4) = −79 ± 11.5 pA/pF. The values of the current recorded at −80, −90, −110, −110, and −120 mV of both HCN1 WT and mutant coexpressed with TRIP8b are significantly higher of the current of HCN1 WT and mutant alone. All values and exact P values are reported in Table 3. **(C)** Mean normalized activation curves of HCN1 WT (black filled circle), HCN1 WT + TRIP8b (1a-4; black open circle), HCN1 NA/DC (red filled circle), and HCN1 NA/DC + TRIP8b (1a-4; red open circle) channels obtained as described in Materials and methods. **(D)** Mean half-activation potential ($V_{1/2}$) of HCN1 WT (black filled circle) = −81.9 ± 1.4 mV; HCN1 WT + TRIP8b (1a-4; black open circle) = −88.6 ± 1.1 mV; HCN1 NA/DC (red filled circle) = −82.4 ± 1 mV; and HCN1 NA/DC + TRIP8b (1a-4; red open circle) = −82.2 ± 1.2 mV. P values are denoted within the scatterplot graph. The number of cells was ≥5. Statistical analysis performed with one-way ANOVA, followed by post-hoc Fisher test.

Table 3. **Mean current density (pA/pF) of HCN1 WT and NA/DC mutant, in the presence and absence of TRIP8b (1a-4), from recordings obtained in cortical neurons from neonatal rats**

V/mV	HCN1 WT	HCN1 WT + TRIP8b	P value	HCN1 NA/DC	HCN1 NA/DC + TRIP8b	P value
−20	0.1 ± 0.3	0.1 ± 0.4	0.14	0.9 ± 1.0	0.7 ± 0.7	4.9E−02
−30	−1.1 ± 0.4	−1.4 ± 0.8	1.4E−03	−0.3 ± 0.6	−0.7 ± 0.6	3.7E−03
−40	−2.0 ± 0.5	−2.3 ± 1.1	2E−05	−0.9 ± 0.4	−1.5 ± 0.6	3.0E−03
−50	−3.3 ± 0.8	−3.3 ± 1.3	2E−04	−1.4 ± 0.4	−2.4 ± 0.9	5.2E−04
−60	−4.7 ± 1.2	−5.8 ± 2.1	6.4E−04	−2.0 ± 0.5	−4.4 ± 1.9	4.2E−05
−70	−6.7 ± 2.0	−10.6 ± 2.9	1.8E−03	−3.0 ± 1.1	−9.1 ± 4.8	4.8E−05
−80	−9.9 ± 2.9	−22.2 ± 5.2	2.3E−03	−6.8 ± 0.6	−18.7 ± 7.3	1.2E−05
−90	−14.1 ± 4.2	−36.2 ± 9.9	3.2E−03	−12.4 ± 5.5	−32.0 ± 9.6	1.7E−05
−100	−18.9 ± 5.5	−48.6 ± 13.7	3.7E−03	−16.3 ± 8.6	−42.2 ± 12.2	2.6E−05
−110	−24.0 ± 7.1	−59.8 ± 16.4	3.1E−03	−19.6 ± 10.5	−52.3 ± 15.6	2.1E−05
−120	−27.2 ± 7.7	−71.6 ± 19.6	6.2E−05	−22.5 ± 12.7	−62.4 ± 19.1	1.7E−05

Data are reported as mean ± SEM. Statistical analysis performed with one-way ANOVA, followed by post-hoc Fisher test.

CNBD of human HCN2 channels (N478D/A479C in human HCN1), which selectively impairs TRIP8b binding to CNBD without affecting cAMP binding and regulation. The behavior of this double mutation has a dual implication: (1) it functionally proves the allosteric model of TRIP8b versus cAMP binding to the CNBD; and (2) it provides a tool for in vivo studies of HCN channels that are fully sensitive to cAMP, without any interference by the TRIP8b auxiliary subunit.

Functional validation of the allosteric regulation of cAMP binding to CNBD by TRIP8b

While the molecular pathway of cAMP potentiation of the HCN channel current is well characterized (Wainger et al., 2001;

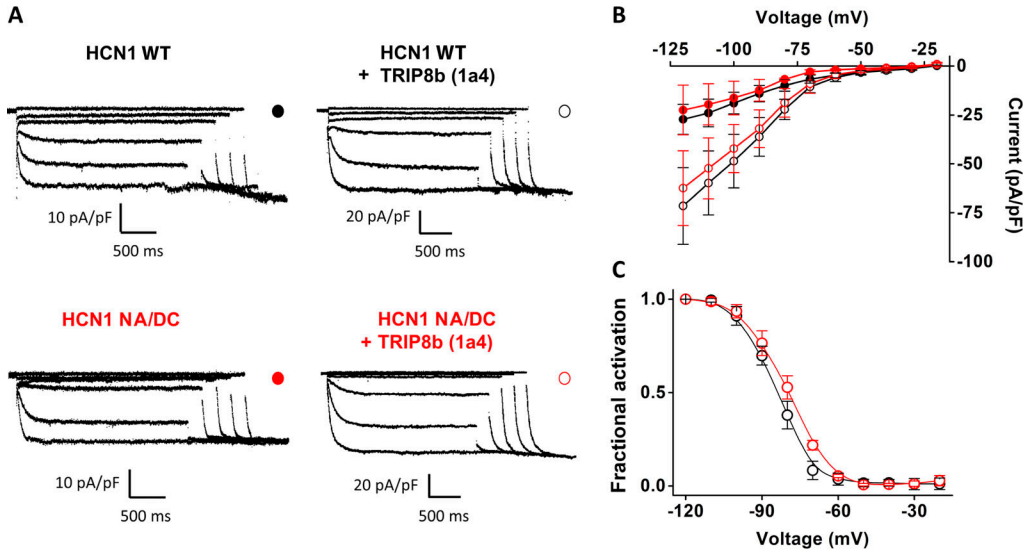

Figure 7. **The NA/DC double mutation prevents TRIP8b regulation of HCN1 gating in cortical neurons derived from hiPSCs. (A)** Representative whole-cell current traces of human HCN1 WT (top) and N478D/A479C (NA/DC) mutant (bottom) recorded in cortical neurons derived from hiPSCs transiently expressing the channels alone (left) or with TRIP8b (1a-4; right) and analyzed as described in Materials and methods. **(B)** Mean current–voltage relationship of HCN1 WT (black filled circle), HCN1 WT + TRIP8b (1a-4; black open circle), HCN1 NA/DC (red filled circle), and HCN1 NA/DC + TRIP8b (1a-4; red open circle). The values of the current recorded at −80, −90, −110, −110, and −120 mV of both HCN1 WT and mutant coexpressed with TRIP8b are significantly higher of the current of HCN1 WT and mutant alone. All values and exact P values are reported in Table 4. Mean current density (pA/pF) measured at −120 mV of HCN1 WT = −27.2 ± 7.7 pA/pF; HCN1 WT + TRIP8b (1a-4) = −71.5 ± 19.5 pA/pF; HCN1 NA/DC = −22.5 ± 12.7 pA/pF; and HCN1 NA/DC + TRIP8b (1a-4) = −62.4 ± 19 pA/pF. In mock-transfected neurons, the current density at −120 mV was −12.5 ± 2 pA/pF, not reported in the graph for the sake of clarity. **(C)** Normalized mean activation curves of HCN1 WT + TRIP8b (1a-4; black open circle) and HCN1 NA/DC + TRIP8b (1a-4; red open circle) channels obtained as described in Materials and methods. Data are presented as means ± SEM. The number of cells was ≥3. Statistical analysis was performed with one-way ANOVA, followed by post-hoc Fisher test.

Table 4. **Mean current density (pA/pF) of HCN1 WT and NA/DC mutant, in the presence and absence of TRIP8b (1a-4), from recordings obtained in cortical neurons derived from hiPSCs**

V/mV	HCN1 WT	HCN1 WT + TRIP8b	P value	HCN1 NA/DC	HCN1 NA/DC + TRIP8b	P value
−20	3.8 ± 1.1	0.4 ± 1.7	0.5	1.4 ± 0.5	1.8 ± 0.9	0.9
−30	0.1 ± 0.8	−3.4 ± 2.2	1.9E−02	−0.5 ± 0.3	−1.2 ± 0.5	0.5
−40	−2.9 ± 1.1	−6.9 ± 3.2	0.1	−1.8 ± 0.5	−3.8 ± 0.6	8E−02
−50	−4.6 ± 1.5	−10.3 ± 4.2	8.6E−02	−3.2 ± 0.7	−6.0 ± 1.0	3.1E−02
−60	−6.8 ± 1.9	−14.0 ± 5.2	4.9E−02	−5.3 ± 1.0	−8.3 ± 1.4	3.4E−02
−70	−11.5 ± 2.7	−22.8 ± 6.2	3.9E−02	−8.6 ± 1.5	−12.3 ± 2.0	4.3E−02
−80	−20.5 ± 5.8	−38.4 ± 8.9	3.5E−02	−13.7 ± 3.1	−22.4 ± 3.5	3.1E−02
−90	−32.9 ± 9.7	−62.8 ± 13.5	2.0E−02	−19.5 ± 6.1	−38.1 ± 5.8	1.3E−02
−100	−43.4 ± 13.5	−88.5 ± 19.1	8.3E−03	−25.4 ± 8.7	−53.2 ± 7.6	7.2E−03
−110	−52.9 ± 17	−112 ± 23.9	4.0E−03	−30.5 ± 10.8	−66.7 ± 9.4	4.8E−03
−120	−57.5 ± 16.3	−132.4 ± 28	2.4E−03	−36.2 ± 10.5	−79.0 ± 11.6	3.0E−03

Data are reported as mean ± SEM. Statistical analysis was performed with one-way ANOVA, followed by post-hoc Fisher test.

Zagotta et al., 2003; Lolicato et al., 2011; Saponaro et al., 2014; Weißgraeber et al., 2017; Gross et al., 2018; Porro et al., 2019), the molecular mechanism of the antagonistic action of TRIP8b on the cAMP effect is still debated.

Previously, we provided biochemical and structural evidence indicating that TRIP8b interacts with two elements of the CNBD: the N-bundle loop and the C-helix (Saponaro et al., 2014, 2018). These findings fit well with the coexistence of both a direct competition and an allosteric inhibition mechanism for the TRIP8b regulation of cAMP binding to the CNBD. This complex mechanism of regulation was previously postulated by us (Hu et al., 2013; Saponaro et al., 2014, 2018) and others (Bankston et al., 2017). Both regulators share the same binding sites on the C-helix, which explains the direct competition model previously supported by several studies (Han et al., 2011; DeBerg et al., 2015; Bankston et al., 2017). On the other hand, the N-bundle loop, which is part of the TRIP8b binding site on the CNBD but also constitutes an allosteric regulative element for cAMP binding (Saponaro et al., 2018), was postulated to be the molecular determinant for allosteric inhibition.

The NA/DC double mutation is located in the N-bundle loop. Functional testing of the NA/DC mutation in the context of the full-length channel in living cells further confirms that TRIP8b allosterically controls cAMP binding by interacting with the N-bundle loop, since cAMP is still able to shift the channel activation curve while the binding of TRP8b to the CNBD is impaired. These experiments represent an important validation for the existence of an allosteric component in the regulation exerted by TRIP8b on cAMP binding.

$HCN_{NA/DC}$ mutants as a tool for in vivo studies of HCN channel regulation

Why is the HCN channel response to cAMP in the nervous system limited by the interaction with TRIP8b? Because TRIP8b is essential for the proper surface expression of HCN channels, simply abolishing TRIP8b expression in vivo through genetic deletion has not allowed such question to be addressed, as knockout of TRIP8b results in drastically reduced HCN channel currents and protein (Lewis et al., 2011). The observation that the NA/DC mutation does not prevent the effects of TRIP8b on channel expression and trafficking means that it may be employed as a genetic tool for dissecting the binary cAMP–TRIP8b regulatory system of HCN channels in the brain. As the sensitivity of neuronal HCN channels to cAMP is critical in several physiological contexts (McCormick and Pape, 1990a, 1990b; Wang et al., 2007; Heys et al., 2010; Marcelin et al., 2012), it would be interesting to determine the consequences of an unabated response of HCN channels to cyclic nucleotides.

For instance, during development, the integrative properties (resonance and temporal summation) of hippocampal CA1 pyramidal neurons display a dorsoventral gradient, which correlates with changes of I_h current properties (Marcelin et al., 2012). In particular, while I_h amplitude increases, its sensitivity to cAMP decreases symmetrically along the dorsoventral axis. Strikingly, these variations match the dorsoventral profile of expression of TRIP8b, and this may potentially explain such variations. However, this tight correlation between hippocampal I_h properties and HCN channels/TRIP8b coexpression has not yet received a conclusive validation. As a consequence, a crucial question concerning the binary TRIP8–cAMP regulation of I_h in hippocampus has also not been addressed either: what is the role of these two opposite gradients of I_h properties (amplitude versus cAMP sensitivity) in the proper development/function of hippocampus? Genetic ablation of TRIP8b cannot answer this question, as it will result in the dissolution of both gradients. In this light, the NA/DC double mutant may represent the resolutive genetic tool approach, as it will selectively impair TRIP8b regulation of the cAMP effect without altering the amplitude gradient of hippocampal I_h.

The $HCN_{NA/DC}$ genetic tool may be similarly critical in understanding the development and function of other cortical regions. Indeed, just like for CA1 pyramidal neurons, the integrative properties of entorhinal cortex layer II stellate cells show a dorsoventral profile of variation, which tightly correlates

with changes in both amplitude and cAMP sensitivity of I_h (Heys et al., 2010). It is thus plausible that I_h currents in several classes of cortical principal cells may be fine-tuned by the binary TRIP8–cAMP regulative system.

Given the fact that hippocampal and entorhinal neurons are both part of the network controlling spatial learning, the NA/DC genetic tool may become crucial in advancing the understanding of I_h and cAMP signaling in the development of spatial memory and navigation.

Acknowledgments

Joseph A. Mindell served as editor.

We thank Prof. Anna Moroni and Dr. Bina Santoro for helpful discussions.

This work was supported by Fondazione Cariplo (grant 2018–0231 to A. Saponaro) and Fondo Ateneo per la Ricerca (grant 2017-ATE-0144 to I. Rivolta).

The authors declare no competing financial interests.

Author contributions: A. Porro performed the experiments and analyzed/interpreted the data; A. Binda performed the experiments and analyzed the data; M. Pisoni performed the experiments and analyzed the data; C. Donadoni performed the experiments and analyzed the data; I. Rivolta contributed to interpretation of the data and revised the manuscript; A. Saponaro conceived the study, performed the experiments and analyzed/interpreted the data, prepared the figures, wrote the manuscript, and coordinated the study.

Submitted: 26 February 2020
Revised: 2 May 2020
Accepted: 8 June 2020

References

Akimoto, M., Z. Zhang, S. Boulton, R. Selvaratnam, B. VanSchouwen, M. Gloyd, E.A. Accili, O.F. Lange, and G. Melacini. 2014. A mechanism for the auto-inhibition of hyperpolarization-activated cyclic nucleotide-gated (HCN) channel opening and its relief by cAMP. *J. Biol. Chem.* 289:22205–22220. https://doi.org/10.1074/jbc.M114.572164

Bankston, J.R., H.A. DeBerg, S. Stoll, and W.N. Zagotta. 2017. Mechanism for the inhibition of the cAMP dependence of HCN ion channels by the auxiliary subunit TRIP8b. *J. Biol. Chem.* 292:17794–17803. https://doi.org/10.1074/jbc.M117.800722

Battefeld, A., N. Rocha, K. Stadler, A.U. Bräuer, and U. Strauss. 2012. Distinct perinatal features of the hyperpolarization-activated non-selective cation current I(h) in the rat cortical plate. *Neural Dev.* 7:21. Available at: https://pubmed.ncbi.nlm.nih.gov/22694806. https://doi.org/10.1186/1749-8104-7-21

Binda, A., A. Panariti, A. Barbuti, C. Murano, R. Dal Magro, M. Masserini, F. Re, and I. Rivolta. 2018. Modulation of the intrinsic neuronal excitability by multifunctional liposomes tailored for the treatment of Alzheimer's disease. *Int. J. Nanomedicine.* 13:4059–4071. https://doi.org/10.2147/IJN.S161563

Bonzanni, M., J.C. DiFrancesco, R. Milanesi, G. Campostrini, B. Castellotti, A. Bucchi, M. Baruscotti, C. Ferrarese, S. Franceschetti, L. Canafoglia, et al. 2018. A novel de novo HCN1 loss-of-function mutation in genetic generalized epilepsy causing increased neuronal excitability. *Neurobiol. Dis.* 118:55–63. https://doi.org/10.1016/j.nbd.2018.06.012

Chen, S., J. Wang, and S.A. Siegelbaum. 2001. Properties of hyperpolarization-activated pacemaker current defined by coassembly of HCN1 and HCN2 subunits and basal modulation by cyclic nucleotide. *J. Gen. Physiol.* 117:491–504. Available at: http://www.jgp.org/lookup/doi/10.1085/jgp.117.5.491. https://doi.org/10.1085/jgp.117.5.491

DeBerg, H.A., J.R. Bankston, J.C. Rosenbaum, P.S. Brzovic, W.N. Zagotta, and S. Stoll. 2015. Structural mechanism for the regulation of HCN ion channels by the accessory protein TRIP8b. *Structure.* 23:734–744. https://doi.org/10.1016/j.str.2015.02.007

DiFrancesco, D.. 1999. Dual allosteric modulation of pacemaker (f) channels by cAMP and voltage in rabbit SA node. *J. Physiol.* 515:367–376. https://doi.org/10.1111/j.1469-7793.1999.367ac.x

Dubé, C.M., A.L. Brewster, and T.Z. Baram. 2009. Febrile seizures: mechanisms and relationship to epilepsy. *Brain Dev.* 31:366–371. https://doi.org/10.1016/j.braindev.2008.11.010

George, M.S., L.F. Abbott, and S.A. Siegelbaum. 2009. HCN hyperpolarization-activated cation channels inhibit EPSPs by interactions with M-type K(+) channels. *Nat. Neurosci.* 12:577–584. https://doi.org/10.1038/nn.2307

Gross, C., A. Saponaro, B. Santoro, A. Moroni, G. Thiel, and K. Hamacher. 2018. Mechanical transduction of cytoplasmic-to-transmembrane-domain movements in a hyperpolarization-activated cyclic nucleotide-gated cation channel. *J. Biol. Chem.* 293:12908–12918. https://doi.org/10.1074/jbc.RA118.002139

Han, Y., Y. Noam, A.S. Lewis, J.J. Gallagher, W.J. Wadman, T.Z. Baram, and D.M. Chetkovich. 2011. Trafficking and gating of hyperpolarization-activated cyclic nucleotide-gated channels are regulated by interaction with tetratricopeptide repeat-containing Rab8b-interacting protein (TRIP8b) and cyclic AMP at distinct sites. *J. Biol. Chem.* 286:20823–20834. https://doi.org/10.1074/jbc.M111.236125

Heys, J.G., L.M. Giocomo, and M.E. Hasselmo. 2010. Cholinergic modulation of the resonance properties of stellate cells in layer II of medial entorhinal cortex. *J. Neurophysiol.* 104:258–270. https://doi.org/10.1152/jn.00492.2009

Hu, L., B. Santoro, A. Saponaro, H. Liu, A. Moroni, and S. Siegelbaum. 2013. Binding of the auxiliary subunit TRIP8b to HCN channels shifts the mode of action of cAMP. *J. Gen. Physiol.* 142:599–612. Available at: http://www.jgp.org/lookup/doi/10.1085/jgp.201311013. https://doi.org/10.1085/jgp.201311013

Lee, C.-H., and R. MacKinnon. 2017. Structures of the Human HCN1 Hyperpolarization-Activated Channel. *Cell.* 168:111–120.e11. https://doi.org/10.1016/j.cell.2016.12.023

Lewis, A.S., E. Schwartz, C.S. Chan, Y. Noam, M. Shin, W.J. Wadman, D.J. Surmeier, T.Z. Baram, R.L. Macdonald, and D.M. Chetkovich. 2009. Alternatively spliced isoforms of TRIP8b differentially control h channel trafficking and function. *J. Neurosci.* 29:6250–6265. https://doi.org/10.1523/JNEUROSCI.0856-09.2009

Lewis, A.S., S.P. Vaidya, C.A. Blaiss, Z. Liu, T.R. Stoub, D.H. Brager, X. Chen, R.A. Bender, C.M. Estep, A.B. Popov, et al. 2011. Deletion of the hyperpolarization-activated cyclic nucleotide-gated channel auxiliary subunit TRIP8b impairs hippocampal Ih localization and function and promotes antidepressant behavior in mice. *J. Neurosci.* 31:7424–7440. Available at: http://www.jneurosci.org/cgi/doi/10.1523/JNEUROSCI.0936-11.2011. https://doi.org/10.1523/JNEUROSCI.0936-11.2011

Li, M., X. Zhou, S. Wang, I. Michailidis, Y. Gong, D. Su, H. Li, X. Li, and J. Yang. 2017. Structure of a eukaryotic cyclic-nucleotide-gated channel. *Nature.* 542:60–65. https://doi.org/10.1038/nature20819

Lolicato, M., M. Nardini, S. Gazzarrini, S. Möller, D. Bertinetti, F.W. Herberg, M. Bolognesi, H. Martin, M. Fasolini, J.A. Bertrand, et al. 2011. Tetramerization dynamics of C-terminal domain underlies isoform-specific cAMP gating in hyperpolarization-activated cyclic nucleotide-gated channels. *J. Biol. Chem.* 286:44811–44820. https://doi.org/10.1074/jbc.M111.297606

Lörincz, A., T. Notomi, G. Tamás, R. Shigemoto, and Z. Nusser. 2002. Polarized and compartment-dependent distribution of HCN1 in pyramidal cell dendrites. *Nat. Neurosci.* 5:1185–1193. https://doi.org/10.1038/nn962

Magee, J.C.. 1998. Dendritic hyperpolarization-activated currents modify the integrative properties of hippocampal CA1 pyramidal neurons. *J. Neurosci.* 18:7613–7624. Available at: http://www.ncbi.nlm.nih.gov/pubmed/9742133. https://doi.org/10.1523/JNEUROSCI.18-19-07613.1998

Magee, J.C.. 1999. Dendritic Ih normalizes temporal summation in hippocampal CA1 neurons. *Nat. Neurosci.* 2:848. https://doi.org/10.1038/12229

Marcelin, B., Z. Liu, Y. Chen, A.S. Lewis, A. Becker, S. McClelland, D.M. Chetkovich, M. Migliore, T.Z. Baram, M. Esclapez, et al. 2012. Dorsoventral differences in intrinsic properties in developing CA1 pyramidal cells. *J. Neurosci.* 32:3736–3747. Available at: http://www.ncbi.nlm.nih.gov/pubmed/22423094%0Ahttp://www.pubmedcentral.nih.gov/articlerender.fcgi?artid=PMC3321843. https://doi.org/10.1523/JNEUROSCI.5870-11.2012

McCormick, D.A., and H.C. Pape. 1990a. Noradrenergic and serotonergic modulation of a hyperpolarization-activated cation current in thalamic

relay neurones. *J. Physiol.* 431:319–342. https://doi.org/10.1113/jphysiol.1990.sp018332

McCormick, D.A., and H.C. Pape. 1990b. Properties of a hyperpolarization-activated cation current and its role in rhythmic oscillation in thalamic relay neurones. *J. Physiol.* 431:291–318. https://doi.org/10.1113/jphysiol.1990.sp018331

Piskorowski, R., B. Santoro, and S.A. Siegelbaum. 2011. TRIP8b splice forms act in concert to regulate the localization and expression of HCN1 channels in CA1 pyramidal neurons. *Neuron*. 70:495–509. https://doi.org/10.1016/j.neuron.2011.03.023

Porro, A., A. Saponaro, F. Gasparri, D. Bauer, C. Gross, M. Pisoni, G. Abbandonato, K. Hamacher, B. Santoro, G. Thiel, et al. 2019. The HCN domain couples voltage gating and cAMP response in hyperpolarization-activated cyclic nucleotide-gated channels. *eLife*. 8. e49672. https://doi.org/10.7554/eLife.49672

Puljung, M.C., H.A. DeBerg, W.N. Zagotta, and S. Stoll. 2014. Double electron-electron resonance reveals cAMP-induced conformational change in HCN channels. *Proc. Natl. Acad. Sci. USA*. 111:9816–9821. https://doi.org/10.1073/pnas.1405371111

Santoro, B., S.G. Grant, D. Bartsch, and E.R. Kandel. 1997. Interactive cloning with the SH3 domain of N-src identifies a new brain specific ion channel protein, with homology to eag and cyclic nucleotide-gated channels. *Proc. Natl. Acad. Sci. USA*. 94:14815–14820. https://doi.org/10.1073/pnas.94.26.14815

Santoro, B., L. Hu, H. Liu, A. Saponaro, P. Pian, R.A. Piskorowski, A. Moroni, and S.A. Siegelbaum. 2011. TRIP8b regulates HCN1 channel trafficking and gating through two distinct C-terminal interaction sites. *J. Neurosci.* 31:4074–4086. Available at: http://www.jneurosci.org/cgi/doi/10.1523/JNEUROSCI.5707-10.2011. https://doi.org/10.1523/JNEUROSCI.5707-10.2011

Santoro, B., R.A. Piskorowski, P. Pian, L. Hu, H. Liu, and S.A. Siegelbaum. 2009. TRIP8b splice variants form a family of auxiliary subunits that regulate gating and trafficking of HCN channels in the brain. *Neuron*. 62:802–813. https://doi.org/10.1016/j.neuron.2009.05.009

Santoro, B., B.J. Wainger, and S.A. Siegelbaum. 2004. Regulation of HCN channel surface expression by a novel C-terminal protein-protein interaction. *J. Neurosci.* 24:10750–10762. https://doi.org/10.1523/JNEUROSCI.3300-04.2004

Saponaro, A.. 2018. Isothermal Titration Calorimetry: A Biophysical Method to Characterize the Interaction between Label-free Biomolecules in Solution. *Bio Protoc*. 8. e2957. https://doi.org/10.21769/BioProtoc.2957

Saponaro, A., F. Cantini, A. Porro, A. Bucchi, D. DiFrancesco, V. Maione, C. Donadoni, B. Introini, P. Mesirca, M.E. Mangoni, et al. 2018. A synthetic peptide that prevents cAMP regulation in mammalian hyperpolarization-activated cyclic nucleotide-gated (HCN) channels. *eLife*. 7. e35753. https://doi.org/10.7554/eLife.35753

Saponaro, A., S.R. Pauleta, F. Cantini, M. Matzapetakis, C. Hammann, C. Donadoni, L. Hu, G. Thiel, L. Banci, B. Santoro, et al. 2014. Structural basis for the mutual antagonism of cAMP and TRIP8b in regulating HCN channel function. *Proc. Natl. Acad. Sci. USA*. 111:14577–14582. https://doi.org/10.1073/pnas.1410389111

Saponaro, A., A. Porro, A. Chaves-Sanjuan, M. Nardini, O. Rauh, G. Thiel, and A. Moroni. 2017. Fusicoccin Activates KAT1 Channels by Stabilizing Their Interaction with 14-3-3 Proteins. *Plant Cell*. 29:2570–2580.

Shah, M.M., Z. Huang, and K. Martinello. 2013. HCN and KV7 (M-) channels as targets for epilepsy treatment. *Neuropharmacology*. 69:75–81. https://doi.org/10.1016/j.neuropharm.2012.03.005

Tsay, D., J.T. Dudman, and S.A. Siegelbaum. 2007. HCN1 channels constrain synaptically evoked Ca2+ spikes in distal dendrites of CA1 pyramidal neurons. *Neuron*. 56:1076–1089. https://doi.org/10.1016/j.neuron.2007.11.015

Wainger, B.J., M. DeGennaro, B. Santoro, S.A. Siegelbaum, and G.R. Tibbs. 2001. Molecular mechanism of cAMP modulation of HCN pacemaker channels. *Nature*. 411:805–810. Available at: http://www.nature.com/doifinder/10.1038/35081088. https://doi.org/10.1038/35081088

Wang, M., B.P. Ramos, C.D. Paspalas, Y. Shu, A. Simen, A. Duque, S. Vijayraghavan, A. Brennan, A. Dudley, E. Nou, et al. 2007. α2A-adrenoceptors strengthen working memory networks by inhibiting cAMP-HCN channel signaling in prefrontal cortex. *Cell*. 129:397–410. https://doi.org/10.1016/j.cell.2007.03.015

Weißgraeber, S., A. Saponaro, G. Thiel, and K. Hamacher. 2017. A reduced mechanical model for cAMP-modulated gating in HCN channels. *Sci. Rep*. 7:40168. https://doi.org/10.1038/srep40168

Williams, S.R., and G.J. Stuart. 2000. Site independence of EPSP time course is mediated by dendritic I(h) in neocortical pyramidal neurons. *J. Neurophysiol*. 83:3177–3182. https://doi.org/10.1152/jn.2000.83.5.3177

Xu, X., Z.V. Vysotskaya, Q. Liu, and L. Zhou. 2010. Structural basis for the cAMP-dependent gating in the human HCN4 channel. *J. Biol. Chem*. 285:37082–37091. https://doi.org/10.1074/jbc.M110.152033

Zagotta, W.N., N.B. Olivier, K.D. Black, E.C. Young, R. Olson, and E. Gouaux. 2003. Structural basis for modulation and agonist specificity of HCN pacemaker channels. *Nature*. 425:200–205. Available at: http://www.nature.com/doifinder/10.1038/nature01922. https://doi.org/10.1038/nature01922

Zhou, L., and S.A. Siegelbaum. 2007. Gating of HCN channels by cyclic nucleotides: residue contacts that underlie ligand binding, selectivity, and efficacy. *Structure*. 15:655–670. https://doi.org/10.1016/j.str.2007.04.012

Supplemental material

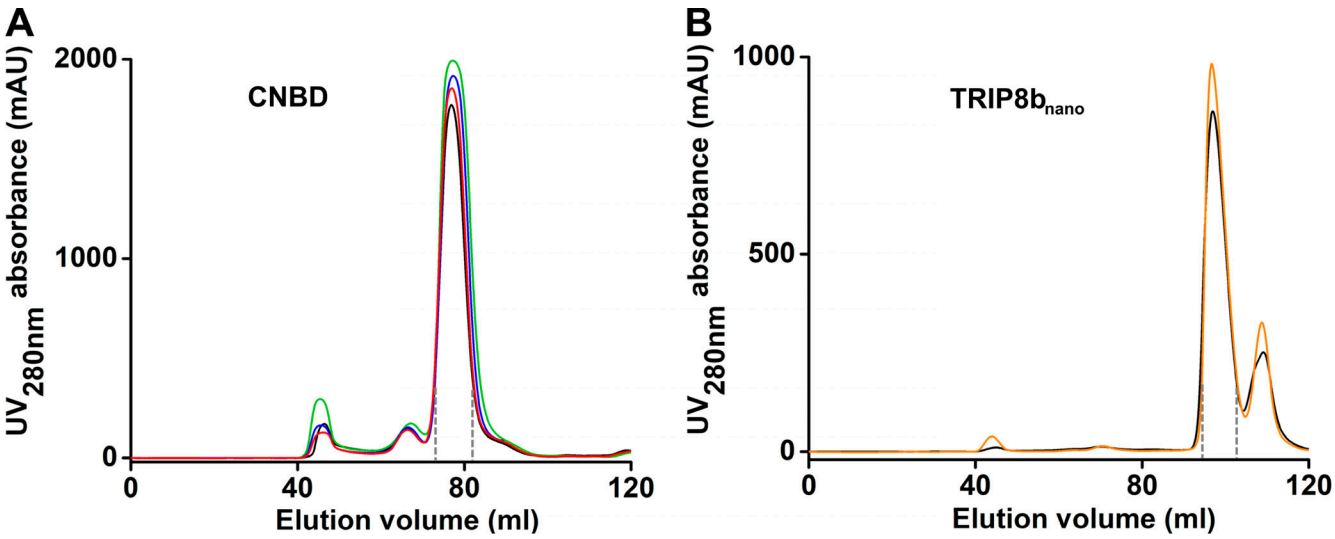

Figure S1. **Biochemical characterization of HCN2 CNBD and $TRIP8b_{nano}$ proteins. (A)** Representative SEC profiles of human HCN2 CNBD WT (black), K666E (red), R650E (blue), and N547D/A548D (green) mutants. **(B)** Representative SEC profiles of $TRIP8b_{nano}$ WT (black) and D252N (orange) mutant. Both CNBD and $TRIP8b_{nano}$ mutant proteins show a symmetrical and monodisperse peak comparable to their respective WT proteins, indicating that mutations did not alter the biochemical features of the proteins. Peak fractions used for the ITC assay are delimited by the gray dotted lines. mAU, milli-arbitrary units.

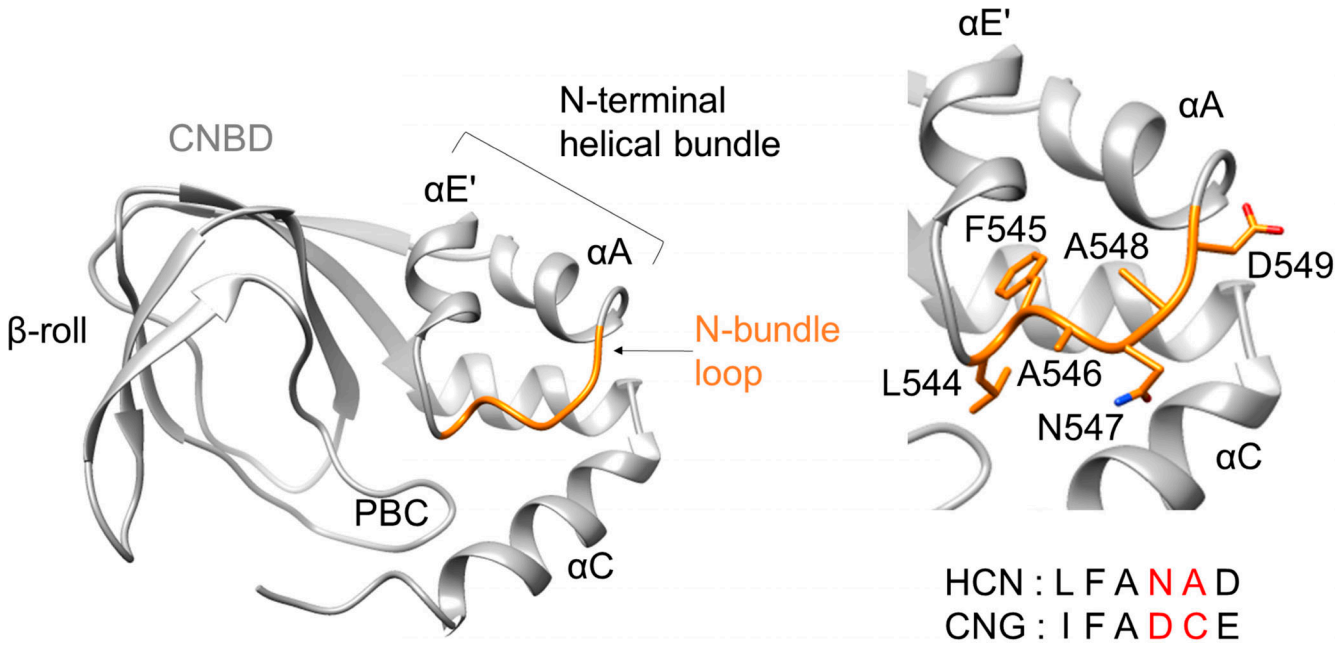

Figure S2. **Structural insights into the N-bundle loop of the CNBD.** Left: Ribbon representation of human HCN2 CNBD structure (cAMP-free conformation; (Saponaro et al., 2014). The main structural elements are labeled, including β-roll; the N-terminal helical bundle, which is composed of α-helices E′ and A (αE′ and αA) interconnected by the N-bundle loop (orange), the phosphate-binding cassette (PBC), and α-helix C. Right: Close-up view showing the residues of the N-bundle loop, labeled in orange. The alignment of the N-bundle loop sequences of mammalian HCN and CNG channels (shown here is CNGA1) is reported below. Nonconservative substitutions are highlighted in red.

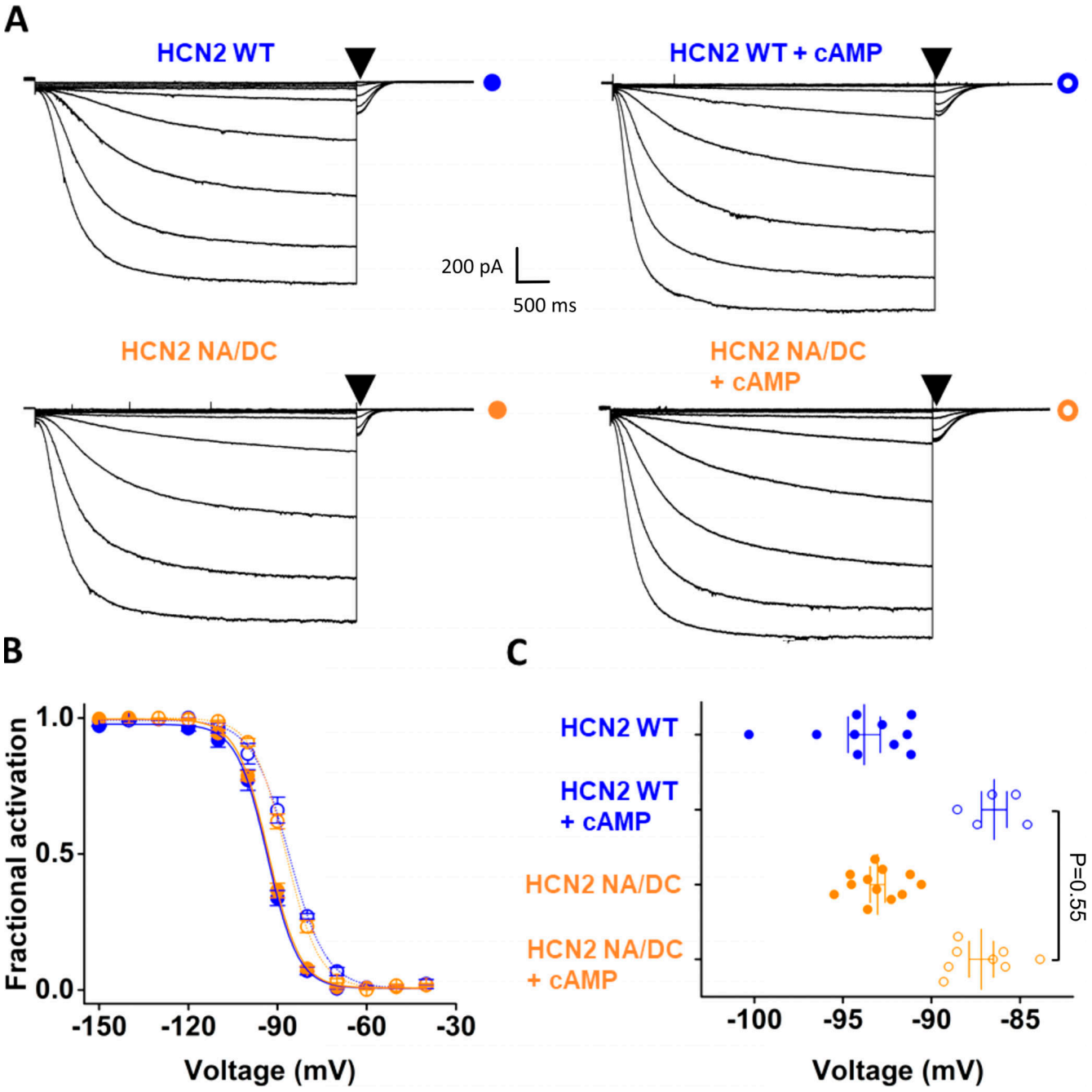

Figure S3. **cAMP sensitivity of HCN2 NA/DC mutant channel. (A)** Representative whole-cell current traces of mouse HCN2 WT (top) and N520D/A521C (NA/DC) mutant (bottom) recorded in HEK 293T cells transiently expressing the channels with control solution (left) or with 1 µM cAMP (right) in the patch pipette. Arrowheads indicate the current selected for analysis in B. **(B)** Normalized mean activation curves of HCN2 WT in control solution (blue filled circle) and cAMP (blue open circle) and of HCN2 NA/DC in control solution (orange filled circle) and cAMP (orange open circle) obtained from tail currents collected at −40 mV (see arrowheads in A). Lines show data fit to a Boltzmann function (see Materials and methods), from which we derived the half-activation potentials ($V_{1/2}$) plotted in C. **(C)** Mean half-activation potential ($V_{1/2}$) of HCN2 WT in control solution (blue filled circle) = −93.8 ± 0.9 mV; HCN2 WT with cAMP (blue open circle) = −86.5 ± 0.7 mV; HCN2 NA/DC in control solution (orange filled circle) = −93 ± 0.4 mV; and HCN2 NA/DC with cAMP (orange open circle) = −87.2 ± 0.7 mV. Data are plotted as dots, and the line represents the mean value ± SEM. The number of cells was ≥5. Statistical analysis performed with one-way ANOVA, followed by post-hoc Tukey test (P values are denoted within the scatterplot graph).